

## Research Article



## OPEN ACCESS

**Received:** Jan 13, 2016  
**Accepted:** Mar 20, 2016

### \*Correspondence to

**Won-Jin Yi**

Department of Oral and Maxillofacial  
Radiology and Dental Research Institute  
Seoul National University School of Dentistry,  
101 Daehak-no, Jongno-gu, Seoul 03080,  
Korea.

E-mail: wjiyi@snu.ac.kr  
Tel: +82-2-2072-3049  
Fax: +82-2-744-3919

Copyright © 2016 Korean Academy of  
Periodontology

This is an Open Access article distributed  
under the terms of the Creative Commons  
Attribution Non-Commercial License (<http://creativecommons.org/licenses/by-nc/3.0/>).

### ORCID

Se-Ryong Kang  
<http://orcid.org/0000-0002-0016-1790>  
Sung-Chul Bok  
<http://orcid.org/0000-0003-0740-9215>  
Soon-Chul Choi  
<http://orcid.org/0000-0002-9846-9936>  
Sam-Sun Lee  
<http://orcid.org/0000-0001-7223-9262>  
Min-Suk Heo  
<http://orcid.org/0000-0003-3406-0645>  
Kyung-Hoe Huh  
<http://orcid.org/0000-0002-8771-0392>  
Tae-Il Kim  
<http://orcid.org/0000-0003-4087-8021>  
Won-Jin Yi  
<http://orcid.org/0000-0002-5977-6634>

<http://jpis.org>

# The relationship between dental implant stability and trabecular bone structure using cone-beam computed tomography

**Se-Ryong Kang,<sup>1</sup> Sung-Chul Bok,<sup>2</sup> Soon-Chul Choi,<sup>2</sup> Sam-Sun Lee,<sup>2</sup> Min-Suk Heo,<sup>2</sup> Kyung-Hoe Huh,<sup>2</sup> Tae-Il Kim,<sup>3</sup> Won-Jin Yi<sup>2\*</sup>**

<sup>1</sup>Department of Biomedical Radiation Sciences, Seoul National University Graduate School of Convergence Science and Technology, Seoul, Korea

<sup>2</sup>Department of Oral and Maxillofacial Radiology and Dental Research Institute, Seoul National University School of Dentistry, Seoul, Korea

<sup>3</sup>Department of Periodontology and Dental Research Institute, Seoul National University School of Dentistry, Seoul, Korea

## ABSTRACT

**Purpose:** The objective of this study was to investigate the relationships between primary implant stability as measured by impact response frequency and the structural parameters of trabecular bone using cone-beam computed tomography(CBCT), excluding the effect of cortical bone thickness.

**Methods:** We measured the impact response of a dental implant placed into swine bone specimens composed of only trabecular bone without the cortical bone layer using an inductive sensor. The peak frequency of the impact response spectrum was determined as an implant stability criterion (SPF). The 3D microstructural parameters were calculated from CT images of the bone specimens obtained using both micro-CT and CBCT.

**Results:** SPF had significant positive correlations with trabecular bone structural parameters (BV/TV, BV, BS, BSD, Tb.Th, Tb.N, FD, and BS/BV) ( $P<0.01$ ) while SPF demonstrated significant negative correlations with other microstructural parameters (Tb.Sp, Tb.Pf, and SMI) using micro-CT and CBCT ( $P<0.01$ ).

**Conclusions:** There was an increase in implant stability prediction by combining BV/TV and SMI in the stepwise forward regression analysis. Bone with high volume density and low surface density shows high implant stability. Well-connected thick bone with small marrow spaces also shows high implant stability. The combination of bone density and architectural parameters measured using CBCT can predict the implant stability more accurately than the density alone in clinical diagnoses.

**Keywords:** Bone and bones; Cone-beam computed tomography; Dental implants; X-ray microtomography

## INTRODUCTION

Primary implant stability is one of the most important factors in the evaluation of successful dental implantation [1,2]. Primary stability at implantation corresponds to a mechanical phenomenon that is relevant to local bone quality and quantity, the type of implant, and the placement technique used [3]. Bone quality is one of the essential factors in predicting

**Funding**

This work was supported by a National Research Foundation of Korea (NRF) grant funded by the Korean government (MEST) (No. 2013R1A2A2A03067942).

**Conflict of Interest**

No potential conflict of interest relevant to this article was reported.

the success rate of implant installation [4,5]. The mechanical competence of bone, which is referred to as bone quality in implant dentistry, comprises bone mass, structural properties, and material properties [6,7]. Consequently, greater failure of implants is likely associated with poor bone mineralization or limited bone resistance on tactile assessment while drilling [8,9].

Quantitative methods for determining implant stability can yield valuable information regarding the success of dental implants [3]. Several methods appropriate for repeated measurements have been developed for the long-term monitoring of implant stability [10-12]. The Osstell Mentor (Integration Diagnostics AB, Goteborgsvagen, Sweden) based on resonance frequency analysis (RFA) measures the stability as an implant stability quotient (ISQ). Generally, local bone density at dental implant recipient sites is measured using computed tomography (CT). The bone density according to CT had significant correlations with insertion torque values and ISQ values, and there was a significant correlation between insertion torque and ISQ values [13]. Bone density obtained using a cone-beam CT (CBCT) showed high correlation with the primary implant stability as assessed by insertion torque and ISQ [14]. The CT numbers according to CBCT and the thickness of cortical bone had strong correlation with ISQ [5,15]. Thus, trabecular bone density and cortical bone thickness are of considerable importance for primary implant stability.

Dental implants are mainly in contact with trabecular bone rather than cortical bone, which directly concerns implant stability [4]. That is, the structure of trabecular bone appears to play a minimal role in primary fixation of an implant, but it is of substantial importance for peri-implant bone healing [15]. Although primary implant stability has been extensively investigated with regard to trabecular bone density and cortical bone thickness, few studies have examined the relationship between implant stability and trabecular bone microstructure. Implant stability according to ISQ showed moderately positive correlation with the stiffness (elastic modulus) of cancellous bone and with the 3D bone-to-implant contact ratio determined by micro-CT [16]. Histomorphometry according to micro-CT showed differences in microstructures of the bone specimens, but none of the trabecular microstructural parameters were significantly correlated with ISQ values. To date, the relationships of implant stability with trabecular bone structural parameters have not been fully explained.

The micro-CT analysis technique has been the prevalent method of measuring 3D trabecular bone microstructures of small samples because of its increased analysis speed compared with conventional histology, its non-invasiveness, and its high spatial resolution [17-20]. However, the application of micro-CT technology to bone analysis is limited to small specimens. Recently, the high correlations between dental CBCT and micro-CT regarding bone structural parameters indicated the possibility of quantifying and monitoring changes of trabecular bone microarchitecture using CBCT clinically [21,22]. However, there have been no studies done on the relationship between primary implant stability and trabecular bone structural parameters using CBCT.

Previously, we developed a new method for evaluating dental implant stability quantitatively using an inductive sensor [23]. The implant stability measured by the impact response frequency showed better differentiability and consistency than did the ISQ value using artificial bone [24]. The objective of this study was to investigate the relationships between primary implant stability measured by impact response frequency and the structural parameters of trabecular bone using CBCT, excluding the effect of cortical bone thickness.

## MATERIALS AND METHODS

We placed 23 dental implants (11.5 mm length and 4.5 mm diameter) (SSII SA Fixture, Osstem Implant, Seoul, Korea) into swine rib bone specimens composed of only trabecular bone without the cortical bone layer. Swine bone samples have been widely used in dental implant experiments. As recommended by the manufacturer, a twist drill with a 2 mm diameter was used to make the initial implant hole, followed by twist drills of 3.0, 3.6, and 4.1 mm in ascending order. After hole preparation, all implants were placed in the hole by a mount driver with the same thread position established in contact with the bone surface. The bone sample with implant was trimmed to a cube of uniform size,  $20 \times 20 \times 20 \text{ mm}^3$ , for micro-CT scanning and stability measurement.

For implant stability measurement, the bone sample was tightly fixed to the specially designed mounting plate using bolts (Figure 1). The system was composed of an analog inductive sensor (Sungjin Corporation, Busan, Korea), an adaptor for amplifying the implant movement, and a signal processing unit [23,24]. A dedicated cube-shaped aluminum adaptor ( $13 \times 13 \times 13 \text{ mm}$ ) was manufactured to amplify the small signal of implant movement. The adaptor, tightly screwed into the implant, was tapped using the tapping rod of the Periostest (Siemens, Bensheim, Germany) as a source of constant excitation force. The inductive sensor detected movement of the adaptor-implant body without physical contact (Figure 2). The interaction between the two magnetic fields of the sensor and adaptor generated an output signal corresponding to the changing distance between the implant and the sensor. The signal from the sensor was digitized at a 1 kHz sampling rate and was high-pass filtered to remove noise. We obtained consecutive impact responses by multiple tapings and calculated the power spectrum of each response by fast Fourier transform (FFT) (Figure 2). The peak frequency of the spectrum was determined as the implant stability (SPF).

We set up a bench-top CBCT system using an X-ray source (SB-80-500, Source-Ray Inc., New York, NY, USA) of 0.04 mm focal spot and a direct-conversion flat panel detector (FLAATZ 330N, DRTECH, Seongnam, Korea). The CBCT images of bone samples with implants in place were obtained at 80 kVp, 0.1 mA, and 1 s with an isotropic voxel size of  $129 \mu\text{m}$ . A total of 320 projection images were recorded at an incremental angle of  $1.125^\circ$  over  $360^\circ$ . The volume image was reconstructed by using the filtered back projection algorithm with a ramp filter. The 3D Laplacian filter and anisotropic diffusion filter were then applied to the reconstructed images for enhancement of the edge-of-bone images. To compare the relationships of trabecular bone structures using CBCT with implant stability to those using micro-CT, micro-CT images of the bone samples were also obtained using a micro-CT scanner (Skyscan 1172, Skyscan, Kontich, Belgium) at 100 kVp, 0.1 mA, and 0.59 s with an isotropic voxel size of  $12.97 \mu\text{m}$ .

The volume images of the samples were exported to CTAn software (Skyscan, Kontich, Belgium) for evaluation of trabecular bone microstructure. The regions of interest (ROI) for CBCT images were selected as an annulus of the inner diameter of 7.1 mm and outer diameter of 9.7 mm around the implant (annulus thickness=1.3 mm) for parameter calculation. The ROI for micro-CT was an annulus of the inner diameter of 4.56 mm and outer diameter of 6.32 mm (annulus thickness=0.88 mm). The following 3D microstructural parameters were calculated for each sample: percent bone volume (BV/TV), bone volume (BV), bone surface (BS), bone specific surface (BS/BV), bone surface density (BS/TV, BSD), trabecular thickness (Tb.Th), trabecular separation (Tb.Sp), trabecular number (Tb.N), trabecular bone pattern

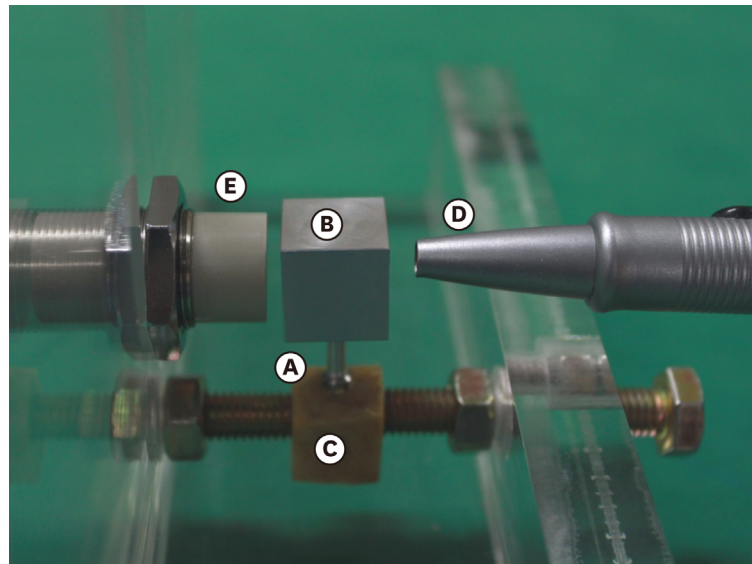


**Figure 1.** Measurement of implant stability in bone samples using an inductive sensor. The implant (A) with an adaptor (B) was placed into the swine bone sample (C) and was tapped using the tapping rod of the Periotest (D). An inductive sensor (E) measured the movement of the implant-adaptor assembly.

factor (Tb.Pf), structural model index (SMI), and fractal dimension (FD). The relationships between SPF and bone microstructural parameters were evaluated using linear regression analysis and Pearson's correlation analysis by SPSS 21 (IBM Corp., Armonk, NY, USA).

## RESULTS

Stability according to peak frequency (SPF) was calculated from impact responses and 3D bone microstructural parameters from micro-CT and CBCT were evaluated for each sample. Figure 2 shows examples of the impact responses, their power spectra, and 3D reconstruction images using micro-CT and CBCT. The power spectra of two bone samples present different SPF values according to the architectural characteristics of the trabecular bone (Figure 2). Table 1 shows means of SPF and microstructural parameters using micro-CT and CBCT for 23 bone samples. Table 2 shows the Pearson's correlation coefficients between SPF values and microstructural parameters using micro-CT (Figure 3) and CBCT (Figure 4). Most of the microstructural parameters showed significant high correlation with SPF in both imaging methods. SPF had a significant positive correlation with BV/TV, BV, BS, BSD, Tb.Th, Tb.N, and FD ( $P < 0.05$  for FD by CBCT,  $P < 0.01$  for others). In contrast, SPF had a significant negative correlation with BS/BV, Tb.Sp, Tb.Pf, and SMI ( $P < 0.05$  for Tb.Sp by CBCT,  $P < 0.01$  for others) (Table 2). SPF had the strongest correlation with BV/TV, BV, and Tb.Pf in both methods. SPF showed a higher correlation with structural parameters using micro-CT than those using CBCT (Table 2).

A linear regression analysis was also conducted to evaluate the relationships between SPF and 3D bone microstructural parameters. Table 3 summarizes the relationships between SPF and bone parameters calculated by both methods. Most parameters had a significant high R<sup>2</sup> measure of goodness of fit ( $P < 0.01$ ), with BV/TV, BV, BS/BV, Tb.Pf, and SMI demonstrating the strongest relationship with SPF. The parameters using micro-CT showed higher goodness of fit than those using CBCT. The stepwise multiple linear regression analysis revealed an increase in

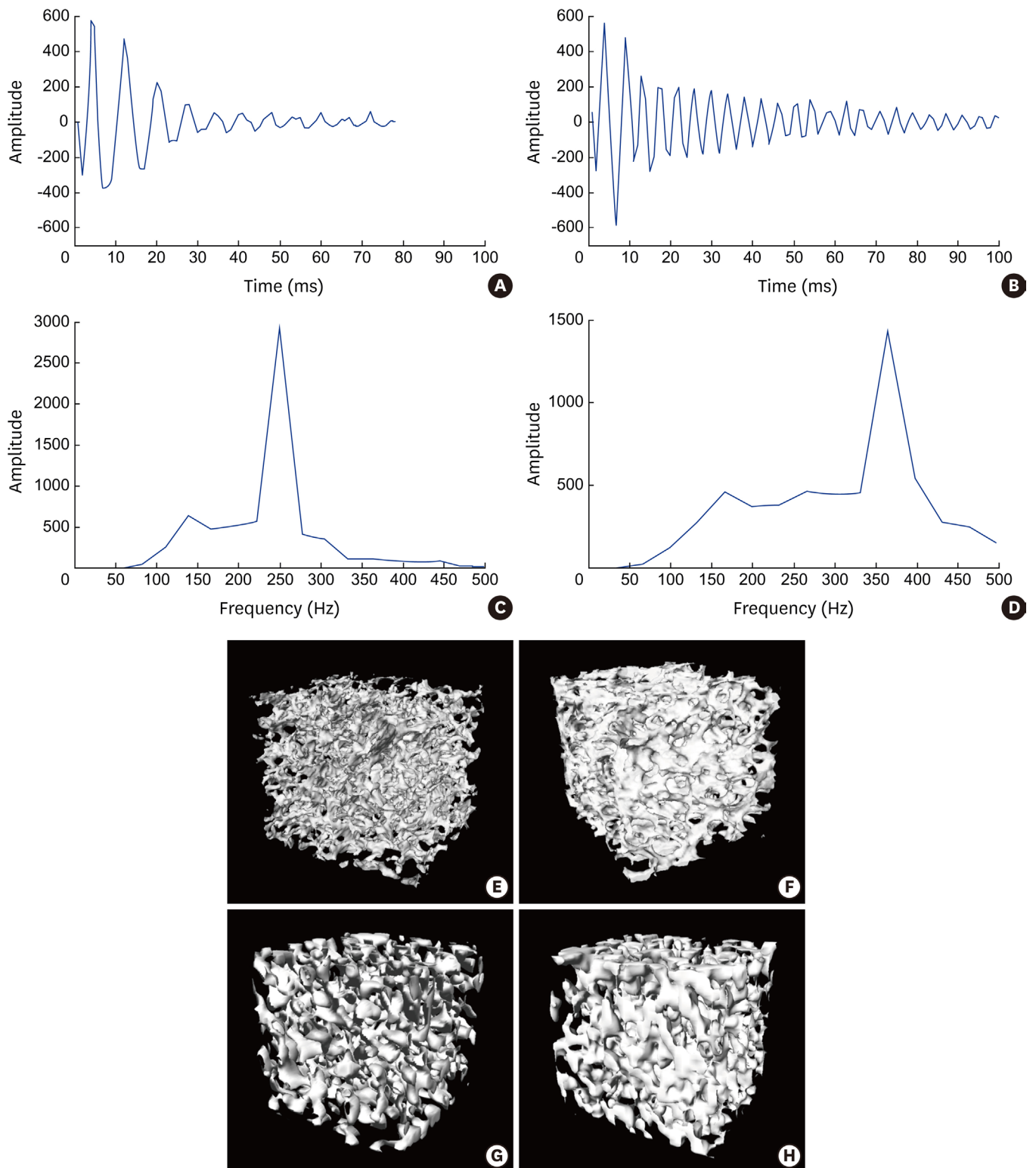


**Figure 2.** Examples of impulse response signals (A, B) and their power spectra (C, D) in two different bone samples, and CT images using micro-CT (E, F) and using CBCT (G, H). The implant (B, D) placed at the bone sample (F, H) with higher volume density and well-connected thick trabeculae shows higher stability than that that (A, C) at the bone sample (E, G).

**Table 1.** Implant SPF (Hz) and 3D bone microstructural parameters using micro-CT and CBCT for 23 implantation samples

|                 | SPF    | BV/TV | BV    | BS     | BS/BV | BSD (BS/TV) | Tb.Th | Tb.Sp | Tb.N | Tb.Pf | SMI  | FD   |
|-----------------|--------|-------|-------|--------|-------|-------------|-------|-------|------|-------|------|------|
| <b>micro-CT</b> |        |       |       |        |       |             |       |       |      |       |      |      |
| Mean            | 315.77 | 27.02 | 9.35  | 402.91 | 43.39 | 11.63       | 0.10  | 0.19  | 2.85 | 7.39  | 2.08 | 2.43 |
| SD              | 37.44  | 3.39  | 1.12  | 33.55  | 3.60  | 0.96        | 0.01  | 0.02  | 0.28 | 2.37  | 0.14 | 0.02 |
| Min             | 223.92 | 18.43 | 6.43  | 331.07 | 36.57 | 9.43        | 0.08  | 0.17  | 2.30 | 3.63  | 1.79 | 2.39 |
| Max             | 374.87 | 33.26 | 11.16 | 465.42 | 51.52 | 13.31       | 0.12  | 0.23  | 3.35 | 14.29 | 2.40 | 2.45 |
| <b>CBCT</b>     |        |       |       |        |       |             |       |       |      |       |      |      |
| Mean            |        | 23.44 | 9.18  | 603.16 | 41.05 | 22.45       | 0.13  | 0.30  | 5.92 | 4.58  | 1.12 | 3.24 |
| SD              |        | 2.33  | 1.70  | 33.48  | 16.45 | 2.87        | 0.02  | 0.01  | 0.59 | 1.47  | 0.12 | 0.44 |
| Min             |        | 17.38 | 5.38  | 531.83 | 59.53 | 17.20       | 0.11  | 0.28  | 4.91 | 2.21  | 0.86 | 2.67 |
| Max             |        | 27.32 | 11.67 | 665.81 | 74.10 | 28.14       | 0.16  | 0.33  | 7.08 | 7.65  | 1.37 | 4.20 |

CBCT, cone-beam computed tomography; SPF, stability according to peak frequency; BV/TV, percent bone volume; BV, bone volume; BS, bone surface; BSD (BS/TV), bone surface density; Tb.Th, trabecular thickness; Tb.Sp, trabecular separation; Tb.N, trabecular number; Tb.Pf, trabecular bone patternfactor; SMI, structural model index; FD, fractal dimension.

**Table 2.** Pearson's correlation coefficients between SPF and bone microstructural parameters using micro-CT and CBCT

|                         | BV/TV | BV   | BS   | BS/BV | BSD (BS/TV) | Tb.Th | Tb.Sp | Tb.N | Tb.Pf | SMI   | FD                 |
|-------------------------|-------|------|------|-------|-------------|-------|-------|------|-------|-------|--------------------|
| <b>micro-CT</b>         |       |      |      |       |             |       |       |      |       |       |                    |
| Correlation coefficient | 0.85  | 0.86 | 0.61 | -0.71 | 0.65        | 0.64  | -0.66 | 0.53 | -0.82 | -0.64 | 0.69               |
| <b>CBCT</b>             |       |      |      |       |             |       |       |      |       |       |                    |
|                         | 0.70  | 0.81 | 0.61 | -0.65 | 0.62        | 0.61  | -0.50 | 0.53 | -0.68 | -0.55 | 0.49 <sup>a)</sup> |

CBCT, cone-beam computed tomography; BV/TV, percent bone volume; BV, bone volume; BS, bone surface; BSD (BS/TV), bone surface density; Tb.Th, trabecular thickness; Tb.Sp, trabecular separation; Tb.N, trabecular number; Tb.Pf, trabecular bone patternfactor; SMI, structural model index; FD, fractal dimension.

<sup>a)</sup>P<0.05, others P<0.01.

the prediction of SPF when bone microstructural parameters were combined (Table 4). Seventy-two percent of the variability in SPF could be accounted for by the BV/TV parameter using micro-CT. Additionally, up to 80% of SPF variability could be accounted for when BV/TV and SMI were used together as predictor variables. On the other hand, up to 71% of SPF variability could be accounted for when BV/TV, BSD, and SMI were used together using CBCT.

## DISCUSSION

Primary implant stability is associated with the mechanical relationship between bone and implant, and secondary implant stability refers to the regeneration of bone following implantation [25,26]. Primary stability is influenced by the quality and quantity of the trabecular bone, implant geometry, and the thickness of the cortical bone [3,27,28]. It is difficult to obtain optimum primary stability from soft bone of low density, and implant failure rates are therefore higher in these cases [29,30]. The noninvasive quantification of implant stability at various points in time provides important information about individualized optimal healing time [31]. The Osstell Mentor system (Integration Diagnostics AB, Goteborgsvagen, Sweden) based on resonance frequency analysis (RFA) provides stability as an implant stability quotient (ISQ). However, some studies have indicated discrepancies between RFA and other stability measurements, such as insertion torque, removal torque, bone mineral density, and histological bone-implant contact [32-34]. In a previous study, we developed a new method for evaluating implant stability quantitatively [23]. The peak frequency of the impact response spectrum was determined as the implant stability criterion (SPF) [24]. The SPF showed a wider dynamic range and higher resolution than the ISQ value in determining dental implant stability in an *in vitro* model [23]. The SPF also revealed better differentiability and consistency with implant stability than did the ISQ value using artificial bone of various densities and thicknesses [24]. Based on these studies, we analyzed the relationships between primary implant stability measured as the SPF and 3D bone architectural parameters using micro-CT and CBCT, excluding the effect of cortical bone thickness.

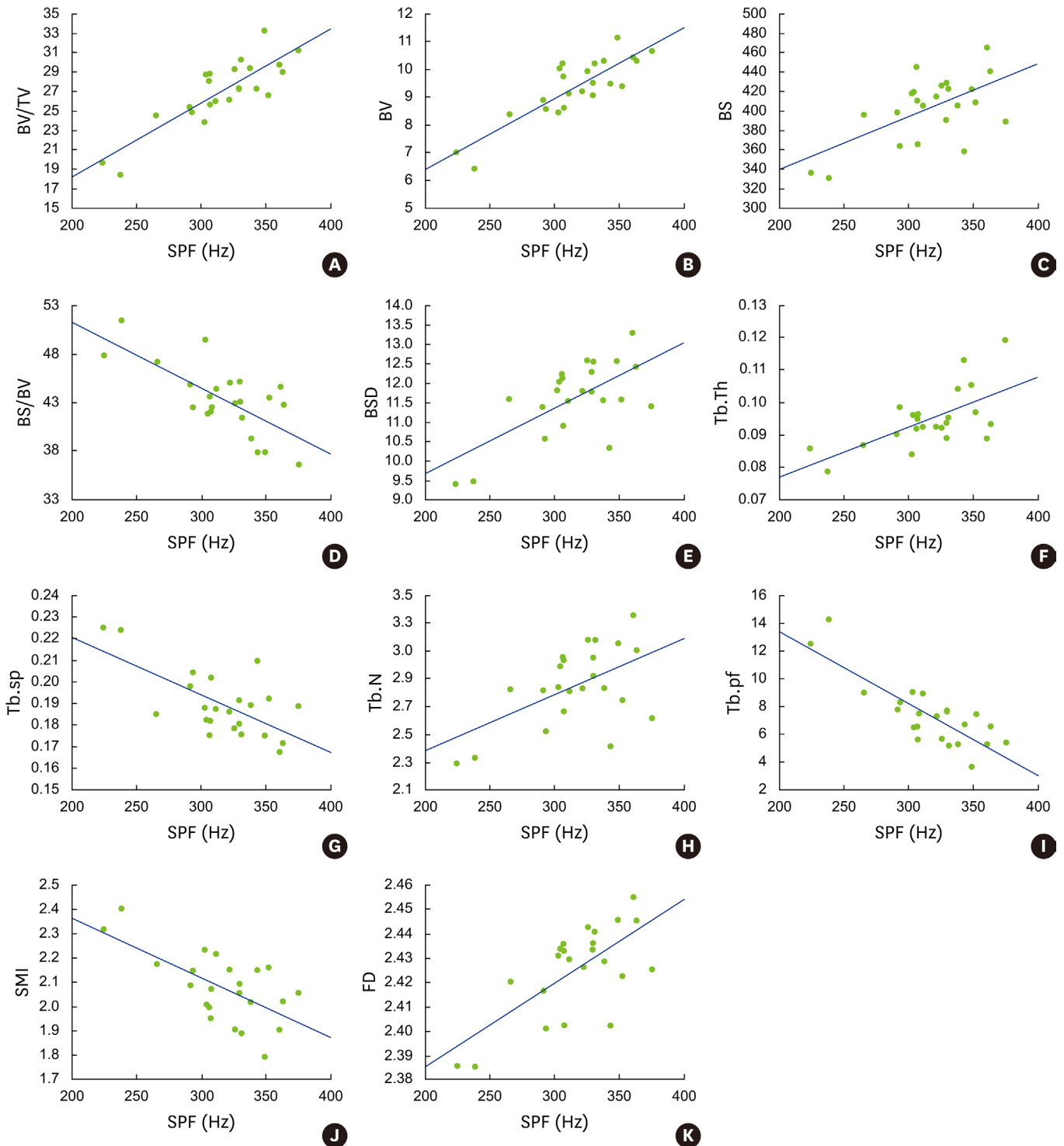


**Figure 3.** Relationships between SPF and 3D bone microstructural parameters of BV/TV (A), BV (B), BS (C), BS/BV (D), BSD (E), Tb.Th (F), Tb.Sp (G), Tb.N (H), Tb.Pf (I), SMI (J), and FD (K) for 23 bone specimens using micro-CT ( $P < 0.01$ ) (SPF, stability according to peak frequency; BV/TV, percent bone volume; BV, bone volume; BS, bone surface; BSD (BS/TV), bone surface density; Tb.Th, trabecular thickness; Tb.Sp, trabecular separation; Tb.N, trabecular number; Tb.Pf, trabecular bone patternfactor; SMI, structural model index; FD, fractal dimension).

Microstructural parameters including BV/TV, BV, BS, BSD, Tb.Th, Tb.N, and FD showed a strong positive correlation with SPF value using both micro-CT and CBCT. On the other

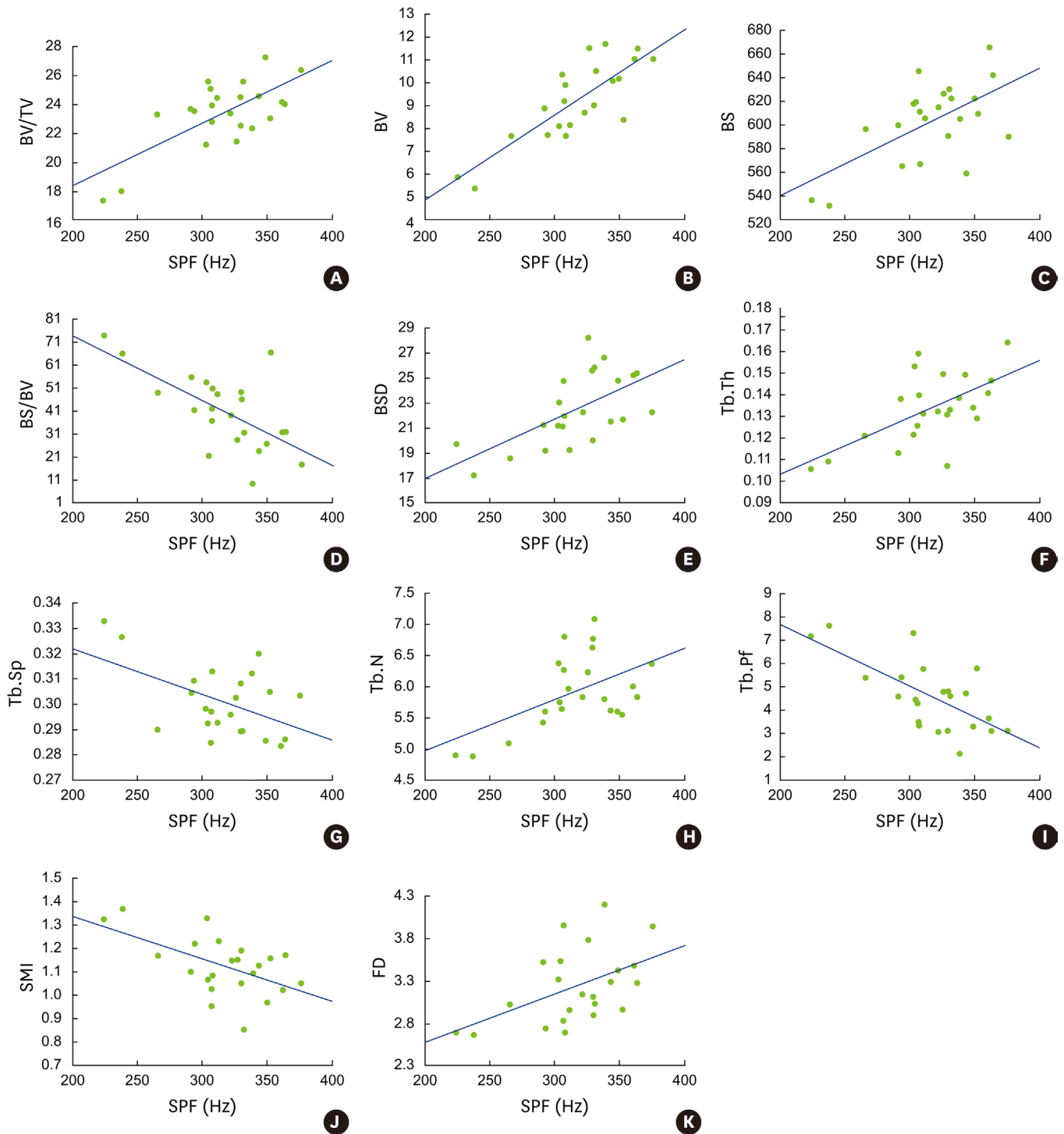


**Figure 4.** Relationships between SPF and 3D bone microstructural parameters of BV/TV (A), BV (B), BS (C), BS/BV (D), BSD (E), Tb.Th (F), Tb.Sp (G), Tb.N (H), Tb.Pf (I), SMI (J), and FD (K) for 23 bone specimens using CBCT ( $P < 0.01$ ,  $P < 0.05$  for Tb.Sp and FD) (SPF, stability according to peak frequency; BV/TV, percent bone volume; BV, bone volume; BS, bone surface; BSD (BS/TV), bone surface density; Tb.Th, trabecular thickness; Tb.Sp, trabecular separation; Tb.N, trabecular number; Tb.Pf, trabecular bone patternfactor; SMI, structural model index; FD, fractal dimension).

hand, SPF had a strong negative correlation with the parameters of BS/BV, Tb.Sp, Tb.Pf, and SMI. The SPF increased when the microstructural parameters of BV/TV, BV, BS, BSD, Tb.Th, Tb.N, and FD increased, while the SPF decreased when BS/BV, Tb.Sp, Tb.Pf, and



**Table 3.** Linear regression analyses between SPF and bone microstructural parameters using micro-CT and CBCT ( $P < 0.01$ )

|                 | BV/TV | BV    | BS    | BS/BV | BSD(BS/TV) | Tb.Th | Tb.Sp | Tb.N | Tb.Pf | SMI   | FD    |
|-----------------|-------|-------|-------|-------|------------|-------|-------|------|-------|-------|-------|
| <b>micro-CT</b> |       |       |       |       |            |       |       |      |       |       |       |
| $R^2$ value     | 0.72  | 0.73  | 0.37  | 0.50  | 0.43       | 0.42  | 0.43  | 0.29 | 0.66  | 0.38  | 0.45  |
| F value         | 52.79 | 57.37 | 12.16 | 21.30 | 15.70      | 14.90 | 15.87 | 8.41 | 43.29 | 14.65 | 19.00 |
| <b>CBCT</b>     |       |       |       |       |            |       |       |      |       |       |       |
| $R^2$ value     | 0.46  | 0.65  | 0.34  | 0.40  | 0.35       | 0.34  | 0.21  | 0.24 | 0.43  | 0.27  | 0.20  |
| F value         | 19.81 | 41.09 | 12.16 | 15.55 | 12.84      | 12.54 | 6.82  | 8.07 | 17.86 | 9.13  | 6.62  |

CBCT, cone-beam computed tomography; SPF, stability according to peak frequency; BV/TV, percent bone volume; BV, bone volume; BS, bone surface; BSD (BS/TV), bone surface density; Tb.Th, trabecular thickness; Tb.Sp, trabecular separation; Tb.N, trabecular number; Tb.Pf, trabecular bone patternfactor; SMI, structural model index; FD, fractal dimension.

SMI increased. The density parameters including BV/TV, BV, BS, and BSD showed positive correlation with the SPF, while BS/BV showed negative correlation with the SPF. BV/TV and BS/BV represent the total volume density of the bone core [35]. BS/BV characterizes the complexity of structures and can be associated with SMI [35]. When BS/BV was low and trabeculae were plate-shaped (low SMI), the SPF was high; however, when BS/BV was high and trabeculae were rod-shaped (high SMI), the SPF was low. On the other hand, when BV/TV was high, the SPF was high, but when BV/TV was low, the SPF was low. We expect that denser bone with high bone volume density and low bone surface density shows high SPF, as the bone has thick trabeculae or a plate-like trabecular pattern [35].

Microstructural parameters such as Tb.Pf, Tb.Th, and Tb.N are associated with the trabecular configuration and 3D organization. Tb.Pf represents inverse trabecular interconnectivity, and a high Tb.Pf value of low trabecular interconnectivity had a low SPF. High Tb.Th of high mean thickness of trabeculae showed a high SPF, and high Tb.N of the reciprocal of the distance between trabecular centers showed a high SPF [35]. High FD providing a statistical index of complexity demonstrated a high SPF. Tb.Sp represents the spacing of bone structures, which is measured as the distance between trabeculae. High Tb.Sp values showed a low SPF, while low Tb.Sp values showed a high SPF. As a result, sparse, thin trabecular bone with large marrow spaces or poorly connected bone showed a low SPF, while well-connected, thick bone with small marrow spaces or trabeculae in close proximity showed a high SPF [35].

The influence of 3D bone microstructural parameters on primary implant stability is not fully understood to date, although one study proposed a correlation between 3D bone microstructural parameters and ISQ values of implant stability. A previous study showed a positive tendency between ISQ value and BV/TV, SMI, BS/BV, TV, BV, and BS and a negative tendency between ISQ value and Tb.Pf, Tb.Th, Tb.N, and Tb.Sp [35]. However, no significant relationships were noted between implant stability and microstructural parameters [35]. Some researchers have reported no significant correlation between bone micro-architectural parameters and ISQ value. One study found no correlation between ISQ value and the

**Table 4.** Stepwise regression analysis with SPF as a dependent variable and bone microstructural parameters using micro-CT and CBCT as independent variables

|                 | Predictors      | Adjusted $R^2$ |
|-----------------|-----------------|----------------|
| <b>micro-CT</b> |                 |                |
| Model 1         | BV/TV           | 0.72           |
| Model 2         | BV/TV, SMI      | 0.80           |
| <b>CBCT</b>     |                 |                |
| Model 1         | BV/TV           | 0.46           |
| Model 2         | BV/TV, BSD      | 0.64           |
| Model 3         | BV/TV, BSD, SMI | 0.71           |

SPF, stability according to peak frequency; CBCT, cone-beam computed tomography; BV/TV, percent bone volume; SMI, structural model index; BSD, bone surface density.

histomorphometric parameters of trabecular bone, such as BV/TV, Tb.Pf, Tb.N, and Tb.Th [15]. Similarly, the ISQ value did not significantly correlate with the histological parameters such as trabecular bone connectivity and volume density [32]. On the other hand, our results demonstrate significant correlation between implant stability and bone microstructural parameters using micro-CT and CBCT, as the SPF from the impact response showed a wider dynamic range and higher resolution than ISQ in determining dental implant stability [23].

Several studies have investigated the relationships between 3D bone micro-architecture and mechanical properties representing failure mechanisms [36-40]. Mechanical properties such as Young's modulus, yield stress, failure load, and insertion torque were measured through mechanical testing [36-40]. Failure load showed significant correlation with structural parameters (Tb.N, Tb.Th, and Tb.Sp) [38], and Young's modulus and yield stress correlated well with BV/TV, BS/BV, and SMI [39,40]. Insertion torque also exhibited significant correlation with BV/TV and SMI [36,37]. These studies confirmed that 3D bone micro-architectural parameters are associated with mechanical properties relative to bone strength. The combination of bone density parameters with micro-architectural parameters showed a higher correlation with mechanical properties and therefore improved the prediction of bone strength [36,37]. These mechanical properties determined by bone strength have a decisive effect on primary implant stability. Consequently, 3D micro-architectural parameters using micro-CT or CBCT, which are correlated with the mechanical properties of bone in relation to bone strength, are significantly correlated with implant stability in this study. Furthermore, there is an increase in implant stability prediction by combining BV/TV and SMI in stepwise forward regression analysis. As a result, the combination of bone density parameters and architectural parameters using micro-CT or CBCT can increase prediction in dental implant stability.

Our study shows that dental implant stability measured by impact response frequency is highly correlated with 3D trabecular microstructural parameters using micro-CT or CBCT. Bone with high volume density and low surface density shows high implant stability, as does well-connected, thick bone with small marrow spaces. The combination of bone density and architectural parameters measured using CBCT can predict the implant stability more accurately than the density alone in clinical diagnoses. In future studies, we will investigate the relationships between implant stability as determined by impact response frequency and microstructural parameters using CBCT in human bones.

## REFERENCES

1. Javed F, Romanos GE. Impact of diabetes mellitus and glycemic control on the osseointegration of dental implants: a systematic literature review. *J Periodontol* 2009;80:1719-30.  
[PUBMED](#) | [CROSSREF](#)
2. Javed F, Romanos GE. The role of primary stability for successful immediate loading of dental implants. A literature review. *J Dent* 2010;38:612-20.  
[PUBMED](#) | [CROSSREF](#)
3. Meredith N. Assessment of implant stability as a prognostic determinant. *Int J Prosthodont* 1998;11:491-501.  
[PUBMED](#)
4. Sakka S, Coulthard P. Bone quality: a reality for the process of osseointegration. *Implant Dent* 2009;18:480-5.  
[PUBMED](#) | [CROSSREF](#)
5. Song YD, Jun SH, Kwon JJ. Correlation between bone quality evaluated by cone-beam computerized tomography and implant primary stability. *Int J Oral Maxillofac Implants* 2009;24:59-64.  
[PUBMED](#)

6. Felsenberg D, Boonen S. The bone quality framework: determinants of bone strength and their interrelationships, and implications for osteoporosis management. *Clin Ther* 2005;27:111.  
[PUBMED](#) | [CROSSREF](#)
7. Bouxsein ML. Bone quality: where do we go from here? *Osteoporos Int* 2003;14 Suppl 5:S118-27.  
[PUBMED](#) | [CROSSREF](#)
8. Friberg B, Sennerby L, Linden B, Gröndahl K, Lekholm U. Stability measurements of one-stage Brånemark implants during healing in mandibles. A clinical resonance frequency analysis study. *Int J Oral Maxillofac Surg* 1999;28:266-72.  
[PUBMED](#) | [CROSSREF](#)
9. van Steenberghe D, Quirynen M, Molly L, Jacobs R. Impact of systemic diseases and medication on osseointegration. *Periodontol 2000* 2003;33:163-71.  
[PUBMED](#) | [CROSSREF](#)
10. Kaneko T. Pulsed oscillation technique for assessing the mechanical state of the dental implant-bone interface. *Biomaterials* 1991;12:555-60.  
[PUBMED](#) | [CROSSREF](#)
11. Kaneko T, Nagai Y, Ogino M, Futami T, Ichimura T. Acoustoelectric technique for assessing the mechanical state of the dental implant-bone interface. *J Biomed Mater Res* 1986;20:169-76.  
[PUBMED](#) | [CROSSREF](#)
12. Noyes DH, Solt CW. Measurement of mechanical mobility of human incisors with sinusoidal forces. *J Biomech* 1973;6:439-42.  
[PUBMED](#) | [CROSSREF](#)
13. Turkyilmaz I, McGlumphy EA. Influence of bone density on implant stability parameters and implant success: a retrospective clinical study. *BMC Oral Health* 2008;8:32.  
[PUBMED](#) | [CROSSREF](#)
14. Isoda K, Ayukawa Y, Tsukiyama Y, Sogo M, Matsushita Y, Koyano K. Relationship between the bone density estimated by cone-beam computed tomography and the primary stability of dental implants. *Clin Oral Implants Res* 2012;23:832-6.  
[PUBMED](#) | [CROSSREF](#)
15. Rozé J, Babu S, Saffarzadeh A, Gayet-Delacroix M, Hoornaert A, Layrolle P. Correlating implant stability to bone structure. *Clin Oral Implants Res* 2009;20:1140-5.  
[PUBMED](#) | [CROSSREF](#)
16. Hsu JT, Huang HL, Tsai MT, Wu AY, Tu MG, Fuh LJ. Effects of the 3D bone-to-implant contact and bone stiffness on the initial stability of a dental implant: micro-CT and resonance frequency analyses. *Int J Oral Maxillofac Surg* 2013;42:276-80.  
[PUBMED](#) | [CROSSREF](#)
17. Kabel J, Odgaard A, van Rietbergen B, Huiskes R. Connectivity and the elastic properties of cancellous bone. *Bone* 1999;24:115-20.  
[PUBMED](#) | [CROSSREF](#)
18. Pothuaud L, Van Rietbergen B, Mosekilde L, Beuf O, Levitz P, Benhamou CL, et al. Combination of topological parameters and bone volume fraction better predicts the mechanical properties of trabecular bone. *J Biomech* 2002;35:1091-9.  
[PUBMED](#) | [CROSSREF](#)
19. Rügsegger P, Koller B, Müller R. A microtomographic system for the nondestructive evaluation of bone architecture. *Calcif Tissue Int* 1996;58:24-9.  
[PUBMED](#) | [CROSSREF](#)
20. Uchiyama T, Tanizawa T, Muramatsu H, Endo N, Takahashi HE, Hara T. A morphometric comparison of trabecular structure of human ilium between microcomputed tomography and conventional histomorphometry. *Calcif Tissue Int* 1997;61:493-8.  
[PUBMED](#) | [CROSSREF](#)
21. Ho JT, Wu J, Huang HL, Chen MY, Fuh LJ, Hsu JT. Trabecular bone structural parameters evaluated using dental cone-beam computed tomography: cellular synthetic bones. *Biomed Eng Online* 2013;12:115.  
[PUBMED](#) | [CROSSREF](#)
22. Panmekiate S, Ngonphloy N, Charoenkarn T, Faruangsang T, Pauwels R. Comparison of mandibular bone microarchitecture between micro-CT and CBCT images. *Dentomaxillofac Radiol* 2015;44:20140322.  
[PUBMED](#) | [CROSSREF](#)
23. Kim DS, Lee WJ, Choi SC, Lee SS, Heo MS, Huh KH, et al. A new method for the evaluation of dental implant stability using an inductive sensor. *Med Eng Phys* 2012;34:1247-52.  
[PUBMED](#) | [CROSSREF](#)

24. Kim DS, Lee WJ, Choi SC, Lee SS, Heo MS, Huh KH, et al. Comparison of dental implant stabilities by impact response and resonance frequencies using artificial bone. *Med Eng Phys* 2014;36:715-20.  
[PUBMED](#) | [CROSSREF](#)
25. Greenstein G, Cavallaro J, Romanos G, Tarnow D. Clinical recommendations for avoiding and managing surgical complications associated with implant dentistry: a review. *J Periodontol* 2008;79:1317-29.  
[PUBMED](#) | [CROSSREF](#)
26. Natali AN, Carniel EL, Pavan PG. Investigation of viscoelastoplastic response of bone tissue in oral implants press fit process. *J Biomed Mater Res B Appl Biomater* 2009;91:868-75.  
[PUBMED](#) | [CROSSREF](#)
27. Bischof M, Nedir R, Szmukler-Moncler S, Bernard JP, Samson J. Implant stability measurement of delayed and immediately loaded implants during healing. *Clin Oral Implants Res* 2004;15:529-39.  
[PUBMED](#) | [CROSSREF](#)
28. Miyamoto I, Tsuboi Y, Wada E, Suwa H, Iizuka T. Influence of cortical bone thickness and implant length on implant stability at the time of surgery--clinical, prospective, biomechanical, and imaging study. *Bone* 2005;37:776-80.  
[PUBMED](#) | [CROSSREF](#)
29. Johns RB, Jemt T, Heath MR, Hutton JE, McKenna S, McNamara DC, et al. A multicenter study of overdentures supported by Brånemark implants. *Int J Oral Maxillofac Implants* 1992;7:513-22.  
[PUBMED](#)
30. Saadoun AP, LeGall ML. Clinical results and guidelines on Steri-Oss endosseous implants. *Int J Periodontics Restorative Dent* 1992;12:486-95.  
[PUBMED](#)
31. Atsumi M, Park SH, Wang HL. Methods used to assess implant stability: current status. *Int J Oral Maxillofac Implants* 2007;22:743-54.  
[PUBMED](#)
32. Huwiler MA, Pjetursson BE, Bosshardt DD, Salvi GE, Lang NP. Resonance frequency analysis in relation to jawbone characteristics and during early healing of implant installation. *Clin Oral Implants Res* 2007;18:275-80.  
[PUBMED](#) | [CROSSREF](#)
33. Ito Y, Sato D, Yoneda S, Ito D, Kondo H, Kasugai S. Relevance of resonance frequency analysis to evaluate dental implant stability: simulation and histomorphometrical animal experiments. *Clin Oral Implants Res* 2008;19:9-14.  
[PUBMED](#)
34. Nkenke E, Hahn M, Weinzierl K, Radespiel-Tröger M, Neukam FW, Engelke K. Implant stability and histomorphometry: a correlation study in human cadavers using stepped cylinder implants. *Clin Oral Implants Res* 2003;14:601-9.  
[PUBMED](#) | [CROSSREF](#)
35. de Oliveira RC, Leles CR, Lindh C, Ribeiro-Rotta RF. Bone tissue microarchitectural characteristics at dental implant sites. Part 1: identification of clinical-related parameters. *Clin Oral Implants Res* 2012;23:981-6.  
[PUBMED](#) | [CROSSREF](#)
36. Ab-Lazid R, Perilli E, Ryan MK, Costi JJ, Reynolds KJ. Pullout strength of cancellous screws in human femoral heads depends on applied insertion torque, trabecular bone microarchitecture and areal bone mineral density. *J Mech Behav Biomed Mater* 2014;40:354-61.  
[PUBMED](#) | [CROSSREF](#)
37. Ab-Lazid R, Perilli E, Ryan MK, Costi JJ, Reynolds KJ. Does cancellous screw insertion torque depend on bone mineral density and/or microarchitecture? *J Biomech* 2014;47:347-53.  
[PUBMED](#) | [CROSSREF](#)
38. Baum T, Carballido-Gamio J, Huber MB, Müller D, Monetti R, Rähn C, et al. Automated 3D trabecular bone structure analysis of the proximal femur--prediction of biomechanical strength by CT and DXA. *Osteoporos Int* 2010;21:1553-64.  
[PUBMED](#) | [CROSSREF](#)
39. Huh KH, Yi WJ, Jeon IS, Heo MS, Lee SS, Choi SC, et al. Relationship between two-dimensional and three-dimensional bone architecture in predicting the mechanical strength of the pig mandible. *Oral Surg Oral Med Oral Pathol Oral Radiol Endod* 2006;101:363-73.  
[PUBMED](#) | [CROSSREF](#)
40. Syahrom A, Abdul Kadir MR, Abdullah J, Öchsner A. Mechanical and microarchitectural analyses of cancellous bone through experiment and computer simulation. *Med Biol Eng Comput* 2011;49:1393-403.  
[PUBMED](#) | [CROSSREF](#)